Toroidal and magnetic Fano resonances in planar THz metamaterials

Srivastava, Yogesh Kumar; Han, Song; Gupta, Manoj; Cong, Longqing; Singh, Ranjan

2017

Han, S., Gupta, M., Cong, L., Srivastava, Y. K., & Singh, R. (2017). Toroidal and magnetic Fano resonances in planar THz metamaterials. Journal of Applied Physics, 122(11), 113105-.

https://hdl.handle.net/10356/86829

https://doi.org/10.1063/1.5001246

Toroidal and magnetic Fano resonances in planar THz metamaterials

Song Han,[1,2] Manoj Gupta,[1,2] Longqing Cong,[1,2] Yogesh Kumar Srivastava,[1,2] and Ranjan Singh[1,2,a)]

[1]*Division of Physics and Applied Physics, School of Physical and Mathematical Sciences, Nanyang Technological University, Singapore, Singapore 637371*

[2]*Centre for Disruptive Photonic Technologies, The Photonics Institute, Nanyang Technological University, 50 Nanyang Avenue, Singapore 639798*

(Received 7 May 2017; accepted 21 August 2017; published online 19 September 2017)

The toroidal dipole moment, a localized electromagnetic excitation of torus magnetic fields, has been observed experimentally in metamaterials. However, the metamaterial based toroidal moment was restricted at higher frequencies by the complex three-dimensional structure. Recently, it has been shown that toroidal moment could also be excited in a planar metamaterial structure. Here, we use asymmetric Fano resonators to illustrate theoretically and experimentally the underlying physics of the toroidal coupling in an array of planar metamaterials. It is observed that the anti-parallel magnetic moment configuration shows toroidal excitation with higher quality (Q) factor Fano resonance, while the parallel magnetic moment shows relatively lower Q factor resonance. Moreover, the electric and toroidal dipole interferes destructively to give rise to an anapole excitation. The magnetic dipole-dipole interaction is employed to understand the differences between the toroidal and magnetic Fano resonances. We further study the impact of intra unit-cell coupling between the Fano resonator pairs in the mirrored and non-mirrored arrangements. The numerical and theoretical approach for modelling the near-field effects and experimental demonstration of toroidal and magnetic Fano resonances in planar systems are particularly promising for tailoring the loss in metamaterials across a broad range of the electromagnetic spectrum. *Published by AIP Publishing.* [http://dx.doi.org/10.1063/1.5001246]

I. INTRODUCTION

The localized torus of magnetic field, known as static toroidal dipole moment, was first introduced by Zel'Dovich in 1958, when he attempted to interpret the parity violation of the interaction between an elementary particle of spin and weak electromagnetic field.[1] The static toroidal dipole does not correspond to any of the well-known electric and magnetic multipoles (dipole, quadrupole, etc.) under the classification of classical electrodynamics, so since earlier times it has been addressed as an "anapole." This excitation was experimentally confirmed by the subsequent measurement of parity non-conservation in the 6S-7S transition of atomic cesium.[2] Since then, the importance of toroidal dipole moment has been widely recognized in nuclear, molecular, atomic, solid state physics, and classical electrodynamics.[3–9] However, the dynamic toroidal moment is less known even though its far-field radiation pattern is indistinguishable from the electric and magnetic dipoles. It was unveiled quite recently by exploiting the idea of artificial electromagnetic metamaterials.[10,11] The solenoid-like configuration formed by discrete split ring resonator (SRR) arrangement allowed for strengthening of the toroidal moment to a detectable level, while simultaneously weakening the electric and magnetic moments.[11–23] It should be noted that these demonstrations of toroidal metamaterials were performed through three-dimensional (3D) structure, which existed only in the microwave frequency range. At higher frequencies, the fabrication of 3D toroidal meta-molecules at the micro and nanoscale is challenging. Therefore, it is necessary to convert the stereoscopic meta-molecules into planar structures for the ease of fabrication.

At terahertz frequencies, the metal-based planar SRR fabricated on a dielectric substrate is considered as the canonical building block of metamaterials. The desired electromagnetic response in the metamaterial is achieved by properly designing its meta-molecules in such a way that the resonantly excited unit cells can be represented in terms of key multipole excitations, such as electric and magnetic dipoles. By tailoring the geometry of the unit cells, metamaterials have supported the well-known Fano resonance excitation with a high Q factor, where an asymmetric SRR with a double gap is excited electromagnetically so that the stimulated current oscillations, which form a closed rectangular loop on the surface of the resonator, establish a time-variant magnetic dipole.[24–26] It is a well-established fact that the magnetic dipole along the wave propagating direction weakly couples to the free space, which fundamentally arises as a high Q Fano resonance. Additionally, the Fano resonance featured by toroidal moment can be excited with an even higher Q factor by just flipping the nearest neighbor Fano resonators under mirror symmetry, i.e., arranging a set of anti-parallel magnetic dipoles.[27–30] However, the physical insight is still unclear and requires a detailed analytical study of the mirrored Fano resonators that have anti-parallel magnetic moments. In addition, the essential distinction also needs to be clarified in terms of lattice distribution for the magnetic and toroidal Fano resonances constructed by a

a)E-mail: ranjans@ntu.edu.sg

two-dimensional array of terahertz asymmetric resonators (TASRs).

To distinguish unambiguously the differences between magnetic and toroidal Fano resonances, we employ two mirrored TASRs for the excitation of toroidal Fano resonance (*t*-Fano) and the corresponding non-mirrored TASRs for the magnetic Fano resonance (*m*-Fano) as shown in Fig. 1. The differences, including the resonant frequencies and *Q* factors between them, will be illustrated by plotting the numerical and experimental results. For the *t*-Fano system, the anti-parallel magnetic dipole-dipole interaction leads to the resonant frequency shift. The observed results are further interpreted by analyzing the theoretically computed multipole components. Since the excitation of toroidal moments depends on the lattice discontinuity (mirror symmetry) of the TASR pair in the unit cell, the center-to-center distance between two TASRs within the unit cell (intra unit cell) is varied to probe the resonance transition and the spectral resonance splitting in the two different systems (mirrored and non-mirrored). By sweeping this parameter, we could clearly observe two additional resonant modes in the non-mirrored configuration that correspond to toroidal Fano resonance at the lowest frequency and an additional magnetic Fano resonance at the higher frequency, while the mirrored system does not undergo any mode splitting and rather shows just a shift in the resonance frequency.

II. DESIGN AND MEASUREMENT

We analyzed the electromagnetic response of an infinite 2D metamaterial array having two different configurations that are classified as type-I and type-II. The unit cell consists of two split ring resonators (TASRs) placed beside each other, where the size (periodicity) of the unit cell is fixed as 160 μm × 80 μm for the type-I system and 150 μm × 75 μm for the type-II system, as shown in Fig. 1. The outer dimension of the individual resonator is 60 μm × 60 μm, strip width of 6 μm, and the split gap size of 3 μm. The center-to-center separation distance between the two resonators is given by *d*, which is varied to probe the near-field coupling. As shown in Fig. 1, *d* is 80 μm for the type-I lattice and 75 μm for the type-II lattice, respectively. The minimum value of *d* can be 60 μm when the resonator pair within the unit cell nearly touches each other along their edge. Similarly, the maximum value of *d* corresponds to a situation where the unit cell resonators are farthest apart with a separation of 100 μm for type-I and 90 μm for type-II, respectively. We stress that the size of the unit cell remains unchanged even when the center to center distance between the TASR pairs is varied within the unit cell. The intra unit cell variation is reflected on the entire metamaterial array. The resonator is made up of 200 nm thick aluminum (Al) metal on a 500 μm thick *p*-type silicon substrate. The asymmetric nature of the square shaped resonator structure is due to the displacement of the split gaps from the center of the resonator. For the type-I resonator, the asymmetry is obtained by displacing *one split gap* on the top by distance of 10 μm away from the center of the resonator. For the type-II resonator, the asymmetry is due to the displacement of *both split gaps* equally by 9 μm from the center of the resonator. Excitation of TASRs with incident electric field being parallel to the non-gap arms leads to a broad symmetric line-shape dipolar resonance and a narrow asymmetric line shaped Fano resonance in the transmission spectra. The numerical simulations were performed by a Finite Integration Technique (FIT) based commercial software, CST Microwave Studio by using a frequency domain solver with plane wave excitation in which the electric field was polarized along the *x*-direction and periodic boundary conditions along the *xy*-plane. After optimizing the parameters, we fabricated the planar metamaterial arrays that consist of two identical Fano meta-molecules in each unit cell on a double side-polished high resistivity silicon, as shown in Fig. 1. The fabrication was performed using conventional photolithography, development, metallization, and lift-off processes. Finally, the electromagnetic response of a set of fabricated samples was measured by a typical 8*f* confocal terahertz time-domain spectroscopy (THz-TDS) system with an operation bandwidth of 0.2 to 2.5 THz. The set up consists of a photoconductive antenna transmitter and

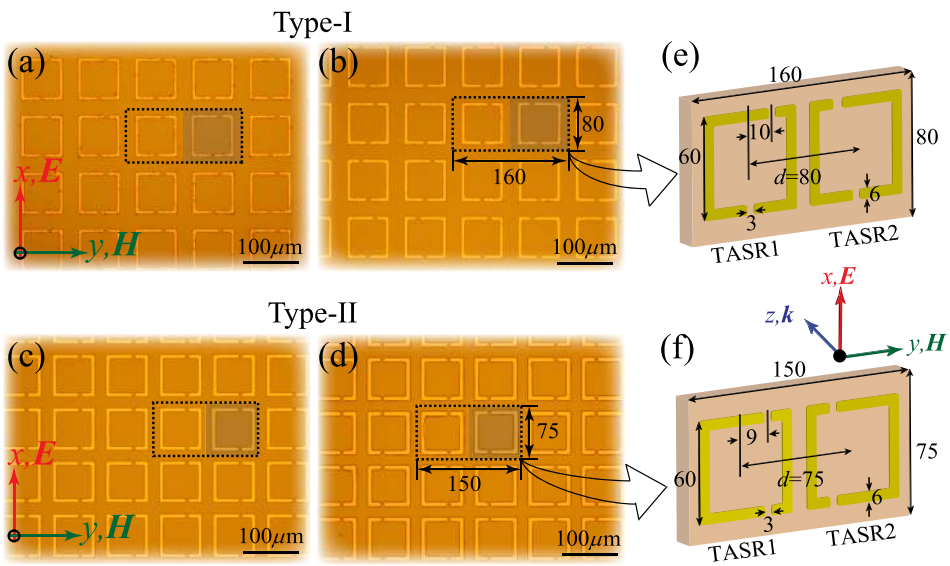

FIG. 1. Schematic of the terahertz asymmetric resonator (TASR) where the meta-molecule under excitation supports magnetic dipole due to a closed current loop on the metal surface. (a), (b) Microscopic image of fabricated samples for type-I Fano and toroidal systems. (c) and (d) Microscopic image of fabricated samples for type-II Fano and toroidal systems. The difference between Fano and toroidal configurations is explained via flipping one of the Fano resonators by 180° (gray area and the corresponding column). (e) and (f) Schematic description of the unit cell with varying "*d*." All dimensions are given in microns.

receiver. A 120-*f*s (pulse duration), 800-nm (wavelength), and 80 MHz (repetition rate) Ti:sapphire oscillating laser beam is used to excite photoconductive GaAs antenna, which generates charged photo carriers. The electrodes with a bias of 70 V are used to accelerate the charge carriers that emit THz electromagnetic radiation. During measurements, the time domain transmitted terahertz signals through the samples were recorded. The time domain signals were transformed to frequency domain and normalized by using an identical bare silicon substrate as the reference by $|\tilde{t}(\omega)| = |\tilde{E}_S(\omega)/\tilde{E}_R(\omega)|$, where $\tilde{E}_S(\omega)$ and $\tilde{E}_R(\omega)$ are the Fourier transformed spectra of the sample and reference, respectively. The measurements were done at room temperature and in a dry nitrogen atmosphere to nullify the effect of water vapor absorption.

III. RESULTS AND DISCUSSION

The measured transmission spectra of the magnetic and toroidal Fano systems are shown in Fig. 2, where we have obtained a good agreement in the transmission intensities between the numerical simulations and the experimental measurements. It is clearly observed that the toroidal system also shows an asymmetric Fano line shape because the individual resonator supports Fano resonance. Due to the excitation mechanism, the Fano resonance in magnetic (non-mirrored) systems is labeled as "*m*-Fano" and such a resonance in mirrored toroidal systems is named "*t*-Fano" resonance. However, the spectra present two clear differences in terms of the resonance frequency and the linewidth of the *m*-Fano and *t*-Fano resonances. First, the resonant frequency of *t*-Fano resonances is lower than that of the corresponding *m*-Fano resonances, where the measured frequency shifts are 73 GHz (simulation: 76 GHz) for the type-I configuration and 84 GHz (simulation: 79 GHz) for the type-II configuration,

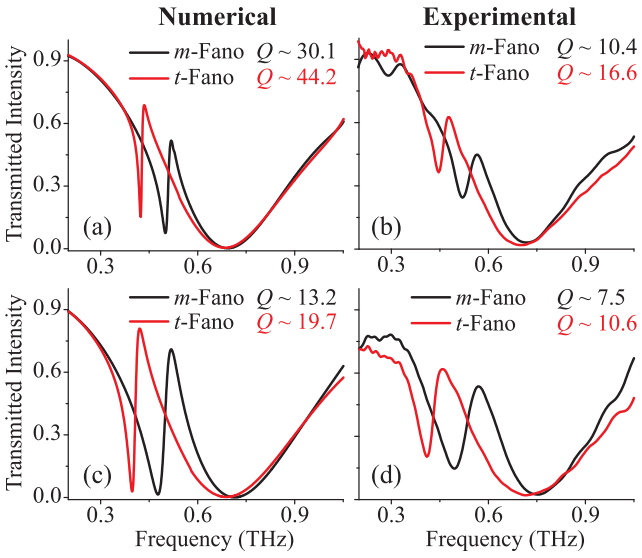

FIG. 2. The spectral comparison between *m*-Fano resonance and *t*-Fano resonance for type-I and type-II configurations. (a) The simulated transmission spectra and (b) the corresponding measured transmission spectra for type-I magnetic and toroidal Fano system. (c) The simulated transmission spectra and (d) the corresponding measured transmission spectra for type-II magnetic and toroidal Fano systems.

respectively. In addition, the Q factor, defined as the ratio of resonance frequency to the resonance linewidth of the transmitted intensity, for the *t*-Fano resonance is overall larger than the corresponding *m*-Fano resonances, where the measured values are 16.6 and 10.6 for *t*-Fano resonances and 10.4 and 7.5 for the corresponding *m*-Fano resonances, respectively. Numerically, these Q factors for *t*-Fano resonances (type-I: $Q = 44.2$, type-II: $Q = 19.7$) and *m*-Fano resonances (type-I: $Q = 30.7$, type-II: $Q = 13.2$) are consistent with the measured results. The measured spectra deviate slightly from the simulated response because of the limited resolution of our measurements and the imperfections in the fabricated samples.

As we have already demonstrated, both *m*-Fano and *t*-Fano resonances generate a group of parallel and anti-parallel magnetic dipoles. Two magnetic dipoles with dipole moments $\vec{m}_1$ and $\vec{m}_2$ interact with each other at center-to-center distance of r, thus the potential energy H of the interaction is given by

$$H = \frac{\mu_0}{4\pi r^3}(\vec{m}_1 \cdot \vec{m}_2 - 3(\vec{m}_1 \cdot \hat{r})(\vec{m}_2 \cdot \hat{r})), \tag{1}$$

where μ_0 is the magnetic permeability and $\hat{r}$ is the unit vector pointing from $\vec{m}_1$ to $\vec{m}_2$. Here, the magnetic dipoles are the same in the proposed systems and they form transverse coupling with each other so that the interaction energy for the parallel coupling is $H_{para} = \frac{\mu_0 m^2}{4\pi r^3}$, while this energy for anti-parallel is $H_{anti} = -\frac{\mu_0 m^2}{4\pi r^3}$. Now, it is clearly illustrated that the *t*-Fano resonance has a lower resonance frequency due to the lower interaction energy of the coupled anti-parallel magnetic dipoles.

The enhancement in the Q factor is intriguing due to the potential applications in biological/chemical sensing, filters, and coherent lasing spasers. Usually, the Q factor in the metamaterial system is limited by the non-radiative losses associated with the dissipative loss and radiative losses due to the geometry and subwavelength size of the meta-molecules. At terahertz frequencies, the Drude metals have extremely high conductivity which nearly eliminates the non-radiative losses such that the radiative losses dominate. Terahertz resonators consisting of two unequal metallic strips form an asymmetric resonator that have been demonstrated in recent years to be an excellent candidate for exciting high Q factor Fano resonance. The high Q resonance in the THz Fano system arises due to the destructive interference between two metallic arms, where the generation of magnetic dipole along the wave propagation direction is weakly coupled to the free space.[24–29] An almost doubled Q factor is observed in the *t*-Fano system compared to the *m*-Fano system. To establish the fact that the enhanced Q factor is due to toroidal moment, we carried out multipole analysis to extract the toroidal component for both Fano and toroidal arrangements, where we extracted the current densities in the resonators through simulations. Then, the multipolar expansions were calculated through the integral of the currents and the corresponding coordinates under the Cartesian basis and the SI units $(\alpha, \beta = x, y, z)$[11–23,27–31]

$$\vec{p}_\alpha = \frac{1}{i\omega}\int J_\alpha d^3 r, \tag{2a}$$

$$\vec{m}_\alpha = \frac{1}{2c}\int [\vec{r}\times\vec{J}]_\alpha d^3r, \tag{2b}$$

$$\vec{m}_\alpha^{(1)} = \frac{1}{2c}\int r^2[\vec{r}\times\vec{J}]_\alpha d^3r, \tag{2c}$$

$$\vec{t}_\alpha = \frac{1}{10c}\int \left[(\vec{r}\cdot\vec{J})r_\alpha - 2r^2J_\alpha\right]d^3r, \tag{2d}$$

$$\vec{t}_\alpha^{(1)} = \frac{1}{28c}\int \left[3r^2J_\alpha - 2r_\alpha(\vec{r}\cdot\vec{J})\right]d^3r, \tag{2e}$$

$$Q_{\alpha\beta}^{(e)} = \frac{1}{i2\omega}\int\left[r_\alpha J_\beta + r_\beta J_\alpha - \frac{2}{3}\delta_{\alpha\beta}(\vec{r}\cdot\vec{J})\right]d^3r, \tag{2f}$$

$$Q_{\alpha\beta}^{(m)} = \frac{1}{3c}\int\left[[\vec{r}\times\vec{J}]_\alpha r_\beta + r_\alpha[\vec{r}\times\vec{J}]_\beta\right]d^3r, \tag{2g}$$

where c is the speed of light and $\vec{r}$ is the displacement vector from the origin to point (x, y, z). The charge conservation relationship $i\omega\rho + \nabla\cdot\vec{J} = 0$ is used to eliminate the charge density (ρ) in favor of current density ($\vec{J}$) in the electric dipole and quadrupole. With the multipole components, electric field (E_S) emitted by the array can be given by[20,27]

$$\vec{E}_S = \frac{\mu_0 c^2}{2\Sigma^2}\left[\begin{array}{l} -ik\vec{p}_\parallel + ik\hat{\Re}\times\left(\vec{m}_\parallel - \frac{k^2}{10}\vec{m}_\parallel^{(1)}\right) - k^2\left(\vec{t}_\parallel + \frac{k^2}{10}\vec{t}_\parallel^{(1)}\right) \\ \\ +k^2\left(Q^{(e)}\cdot\hat{\Re}\right) - \frac{k^2}{2}\hat{\Re}\times\left(Q^{(m)}\cdot\hat{\Re}\right) \end{array}\right] \times\exp(ik\Re), \tag{3}$$

where k is the wave number, the subscript $(\cdots)_{//}$ denotes the projection of the vector into the plane of the array, μ_0 is the vacuum magnetic permeability, Σ^2 denotes the area of the unit cell, $\Re$ is the perpendicular distance of the observer from the planar array, and $\hat{\Re}$ is the unit vector perpendicular to the plane of array. Equation (3) allows us to calculate the electric field emitted by an infinitely large two-dimensional array of meta-molecules. The terms that contribute to the emitted field in Eq. (3) are the electric ($\vec{p}$), magnetic ($\vec{m}$), and toroidal ($\vec{t}$) dipoles, electric quadrupole ($Q^{(e)}$), magnetic quadrupole ($Q^{(m)}$), and the so-called mean-square radii of toroidal ($\vec{t}^{(1)}$) and magnetic ($\vec{m}^{(1)}$) dipoles, which are the lowest-order corrections retained to account for the finite size of the meta-molecules.[20,27] The higher order multipoles, such as toroidal quadrupole and electric and magnetic octupoles, have been omitted due to their extremely low contributions. Therefore, the radiation reflected and transmitted by the 2D array can be found from

$$\vec{E}_{reflected} = \left[\vec{E}_S\right]_{\hat{\Re}=-\hat{k}}, \tag{4}$$

$$\vec{E}_{transmitted} = \left[\vec{E}_S\right]_{\hat{\Re}=\hat{k}} + \vec{E}_{incident}, \tag{5}$$

where $\pm\hat{k}$ indicates the unit vectors in the direction of the propagating plane wave and the corresponding opposite direction. Therefore, the reflection and transmission as well as the scattering intensities of multipole components (x-polarized electric dipole p_x and t_x, z-directed magnetic dipole m_z, and magnetic quadrupole $Q^{(m)}$) are thus normalized by the incident electric field, as shown in Fig. 3. Overall, the scattering of electric dipole dominates the radiation so that the scattered spectrum of electric dipole almost overlaps with the reflection spectrum, while the enhancement of magnetic dipoles along the propagation direction or toroidal dipole which opposes the electric dipole would mediate the Fano resonance and the resonant Q factor, as we have clearly illustrated here. From Figs. 3(a) and 3(c), the analyzed multipole scattering corresponds to the Fano system where only the magnetic dipole is strongly enhanced at the m-Fano resonance. From the scattered intensities of the multipoles as shown in Figs. 3(b) and 3(d), the toroidal dipole at the t-Fano resonance is strongly enhanced for x-axis polarization and the excited toroidal dipole is oriented along the x-direction as well.

A distinctive feature of the toroidal dipole is its ability to radiate with the same angular momentum as the electric dipole. Indeed, consider the toroidal and electric dipoles placed at the origin ($r = 0$), one obtains the radiated electric and magnetic fields due to the superposition of the two dipoles

$$\begin{aligned}\vec{E}_{tot} &= \vec{E}_p + \vec{E}_t \\ &= \left[\frac{\left(\vec{r}\cdot\left(\vec{p} - ik\vec{t}\right)\right)F(\omega,r)}{c^2r^2}\vec{r} - \frac{G(\omega,r)}{c^2r^2}\left(\vec{p} - ik\vec{t}\right)\right] \\ &\quad\times\frac{\exp(-ikr + i\omega t)}{r},\end{aligned} \tag{6}$$

$$\begin{aligned}\vec{H}_{tot} &= \vec{H}_p + \vec{H}_t \\ &= -\frac{ikD(\omega,r)}{cr}\left[\vec{r}\times\left(\vec{p} - ik\vec{t}\right)\right]\frac{\exp(-ikr + i\omega t)}{r},\end{aligned} \tag{7}$$

where D, F, and G are functions given by Ref. 17. It is observed from Eqs. (6) and (7) that both electric and magnetic fields vanish in the case of $\vec{P} = ik\vec{T}$ (equal amplitude and out-of-phase), which indicates a complete destructive interference (anapole) of toroidal and electric dipole moments everywhere except at $r = 0$. For this specific case, the system tightly traps incident fields so that it presents a non-radiative configuration and its resonance has the maximum Q factor.[17,31] In our system, the toroidal excitation is highly enhanced but always remains weaker than the excitation of the electric dipole. However, the phase difference between the scattered electric dipole and toroidal dipole is π at the Fano resonance frequency, as shown by black stars in Fig. 4. This indicates that the proposed planar toroidal system still supports anapole like excitation due to the destructive interference between toroidal and electric dipoles that gives rise to a higher Q factor resonance. Therefore, the maximum Q factor could be obtained if a perfect destructive interference occurs, i.e., perfect anapole scenario, which would result from enhancement of the strength of toroidal excitation.[17,31] However, the strength of the toroidal dipole remains weak in the planar metamaterial design.

So far, we have clearly demonstrated that it is the excitation of toroidal moments that leads to the larger Q factor resonance in the metamaterial system. The t-Fano resonances

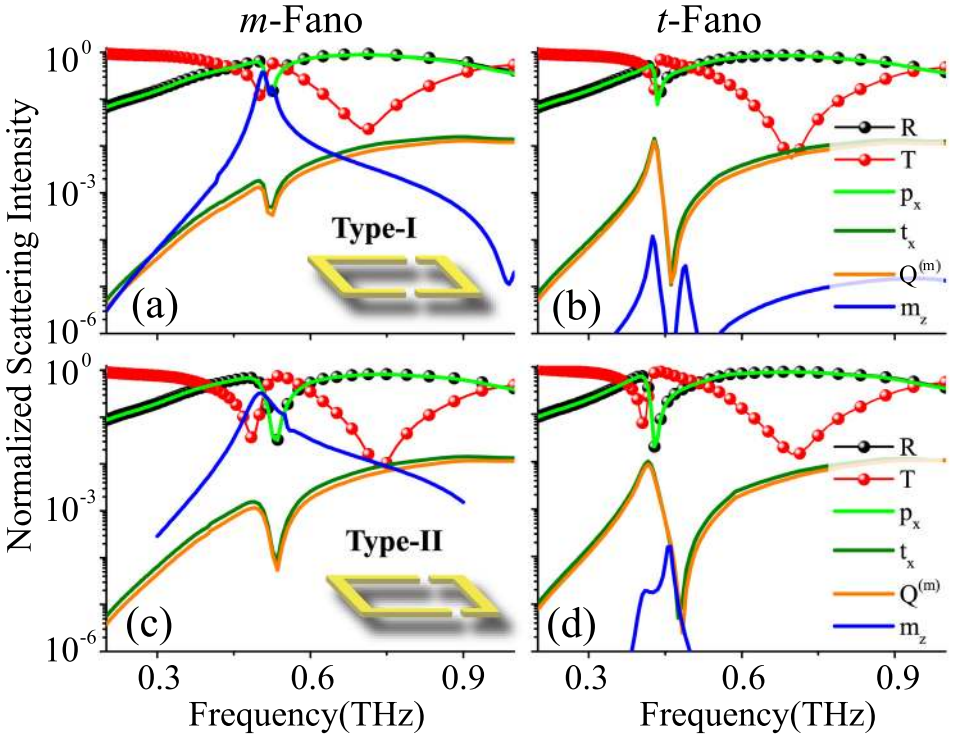

FIG. 3. Calculated reflection (R), transmission (T), and normalized multipole excitation in the planar metamaterial. Normalized far-field scattering of different multipoles for (a) type-I *m*-Fano system and (b) type-I *t*-Fano system, (c) type-II *m*-Fano system and (d) type-II *t*-Fano system.

are excited due to arrangement of resonant Fano (*m*-Fano) meta-atoms, while the excitation of toroidal moment only depends on the head-to-tail configuration of magnetic dipoles. Then, we further investigate the intrinsic differences between the magnetic and toroidal Fano resonances by varying the center-to-center spacing between the meta-molecules of *m*-Fano and *t*-Fano systems. As shown in Fig. 1, each unit cell comprises two TASRs. A TASR behaves as a radiatively damped resonator which is driven by the incident field and the fields emitted by all other TASRs in the system.[24–29,32–36] We probe the impact of coupling by varying the center-to-center distance d between the TASR pairs, while the size of the unit cell is kept constant.

Figures 5(a) and 5(c) show simulated transmission spectra of the non-mirrored *m*-Fano system for type-I (lower asymmetry) and type-II (higher asymmetry) configurations as a function of center-to-center distance d, where two resonant modes (II and IV) always exist, while two other modes (I and III) disappear for certain values of d. The simulated transmission and surface current distributions at these resonant modes for different values of d are shown in Figs. 6(a) and 6(b), respectively. The 2nd (II) and 4th (IV) branches correspond to the intrinsic Fano resonance and electric dipole resonance of an individual TASR which remains excited in the system. Two new modes, i.e., 1st (I) resonance and 3rd (III) resonance, appear when the Fano TASRs are close to each other where the resonant modes are mainly mediated by the coupling between the TASR pairs. In fact, these two split modes arise when two asymmetric meta-atoms are brought very close to each other ($d < 75\,\mu$m and $d > 85\,\mu$m for type-I system), where they support simultaneous excitation of the symmetric and anti-symmetric resonances.[37] Surprisingly, the 1st mode (I) corresponds to a toroidal resonance as revealed by the surface currents in Fig. 6(b), where the two TASRs support opposing magnetic moments.[27] The 3rd mode is a Fano resonance mode that arises due to the near field coupling between the closest metallic strips of TASR1 and TASR2, as shown by the dotted rectangular box in Fig. 6(b).

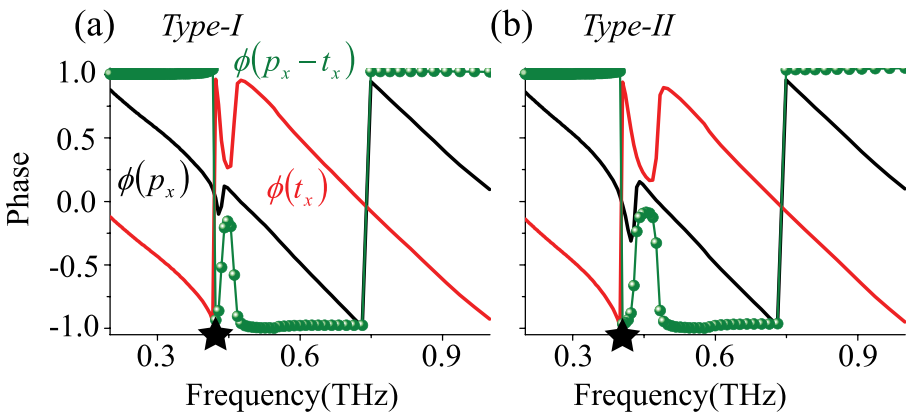

FIG. 4. Numerically calculated phase of the electric dipole (Black line), toroidal dipole (Red line), and the phase difference between them (Olive line). (a) type-I toroidal system and (b) type-II toroidal system. The black stars indicate that the phase difference is 180°, i.e., the excited toroidal dipole is anti-parallel to the electric dipole which is a signature of an anapole excitation.

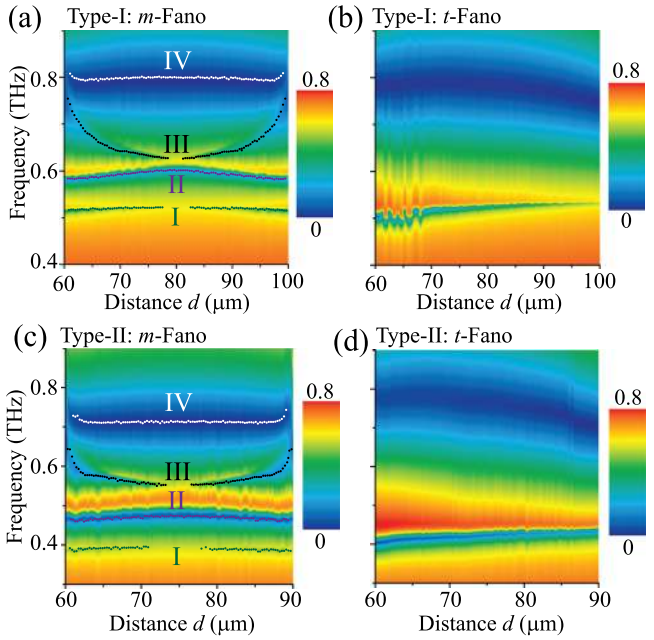

FIG. 5. Simulated transmission spectra for the *m*-Fano and *t*-Fano metamaterials by changing the center-to-center distance *d* of two TASRs.

Similarly, the transmission spectra of the mirrored *t*-Fano system of type I (lower asymmetry) and II (higher asymmetry) are shown in Figs. 5(b) and 5(d) as a function of separation distance between the mirrored TASR pair. The spectra show that there are only two resonant modes corresponding to the intrinsic Fano resonance at lower frequency and electric dipole resonance at higher frequency where the resonant frequencies shift when the center-to-center distance *d* of two mirrored TASRs is varied. In the mirrored toroidal system, the two resonances remain unchanged and do not show any mode splitting behavior. The *t*-Fano resonance spectra and dipole resonances along with surface current distribution at Fano resonance are shown in Fig. 7. The surface currents on the two mirrored TASRs are equivalent to two groups of anti-parallel magnetic dipoles (interaction energy $H_{anti} = -\frac{\mu_0 m^2}{4\pi r^3}$) for different distances *d*. The interaction energy at the *t*-Fano resonance is always described as a group of anti-parallel magnetic dipole-dipole interactions, where the magnetic dipoles generated by Fano meta-molecules are identical. For the distance $d = 60\,\mu$m, the surface currents on two asymmetric TASRs are comparable so that the interaction energy is approximated as $H_{anti} = -\frac{\mu_0 m^2}{4\pi r^3}$, i.e., the dipole-dipole distance *r* is approximately equal to 60 μm. This leads to the highest resonant frequency. With the increase in *d*, the surface currents asymmetrically distribute on two asymmetric meta-atoms, where the longer TASR arm accumulates more surface currents so that the induced magnetic dipoles move to the sides of the longer arms of meta-atoms, as shown in Fig. 7(b). This indicates that the dipole-dipole distance *r* is always shorter than the case of $d = 60\,\mu$m. As a result, the interaction energy continuously

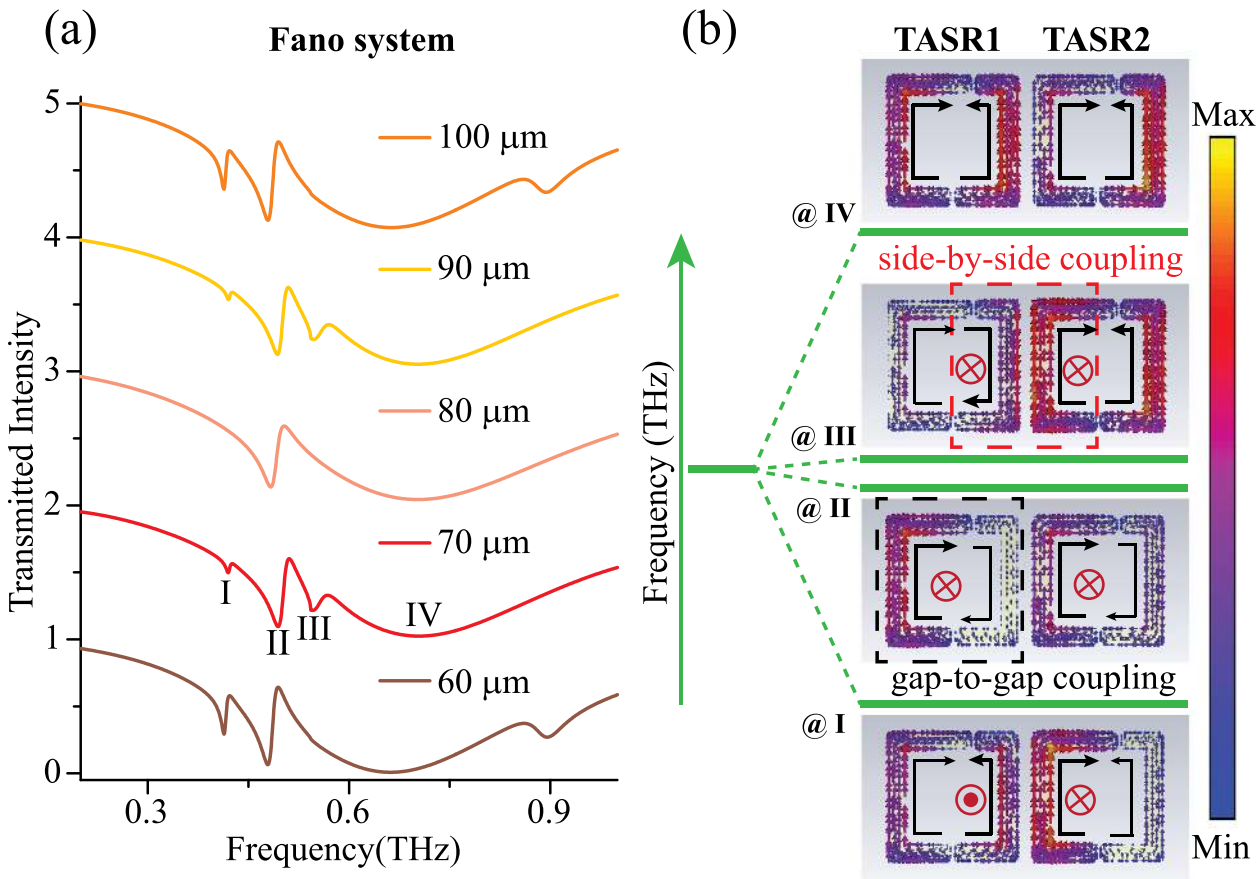

FIG. 6. (a) Simulated transmission intensities of the *m*-Fano metamaterials by changing the center-to-center distance, *d* of two TASRs. (b) Surface current distributions at the corresponding resonances I (new toroidal mode), II (gap-to-gap Fano coupling), III (side-by-side Fano coupling), and IV (electric dipole mode), respectively.

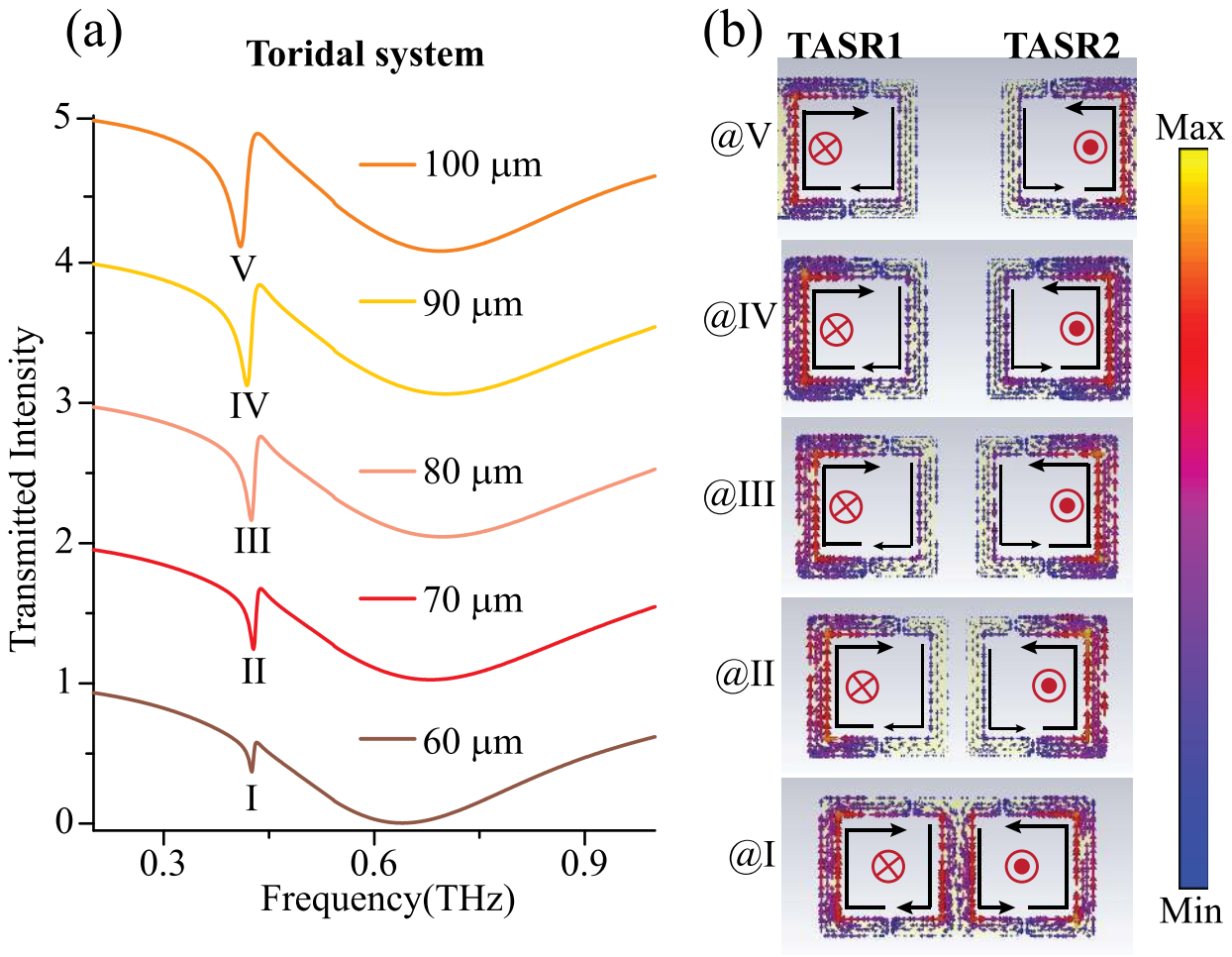

FIG. 7. (a) Simulated transmission intensities of *t*-Fano metamaterials by changing the center-to-center distances of two TASRs. (b) Surface current distributions at the toroidal resonances I, II, III, IV, and V, respectively.

decreases so that the toroidal resonant frequency gradually red-shifts with the increase in d.

IV. CONCLUSIONS

In conclusion, we have investigated toroidal and magnetic Fano resonances in planar terahertz metamaterial arrays. The mirrored toroidal resonances (*t*-Fano resonances) showed significant enhancement in Q factors compared to the non-mirrored magnetic (*m*-Fano resonance) Fano resonance. We have experimentally demonstrated that the toroidal moment plays an important role in the line narrowing of the Fano resonances, which would enhance the performance in terms of Q factor of metamaterial based photonic devices. Compared to the *m*-Fano resonances, the enhanced Q factor of the *t*-Fano resonance comes from the relatively superior non-radiative configuration of an anapole due to the destructive interference between the toroidal and the electric dipoles. The frequency shift of *t*-Fano resonance has been illustrated as two coupled magnetic dipole-dipole interactions, where the interaction energy has confirmed that these mechanisms can qualitatively predict the resonance frequency shifts. We also probed the intra unit cell coupling between the Fano resonator pair in the non-mirrored magnetic Fano configuration as well as the mirrored toroidal Fano configuration. The magnetic Fano arrangement showed mode splitting behavior unlike the mirrored configuration where we only observed the enhancement of Q factor of the Fano resonance. Overall, the high Q factor anapole like resonances presented here could be exploited for metamaterial applications in ultrasensitive sensing, lasing spasers, modulators, narrowband filters, and nonlinear optics.

SUPPLEMENTARY MATERIAL

See supplementary material for the information on the extraction of the resonance Q-factor by using the Fano model.

ACKNOWLEDGMENTS

The authors gratefully acknowledge the Singapore Ministry of Education (MOE) Grant No., MOE2015-T2-2-103 for funding of this research.

[1]I. B. Zel'Dovich, Sov. Phys. - JETP **6**, 1184 (1958).
[2]M. C. Noecker, B. P. Masterson, and C. E. Wieman, Phys. Rev. Lett. **61**, 310 (1988).
[3]V. V. Flambaum and D. W. Murray, Phys. Rev. C **56**, 1641 (1997).
[4]V. V. Flambaum and I. B. Khriplovich, Sov. Phys. - JETP **52**, 835 (1980).
[5]A. Ceulemans and L. F. Chibotaru, Phys. Rev. Lett. **80**, 1861 (1998).
[6]G. N. Afanasiev, J. Phys. D: Appl. Phys. **34**, 539 (2001).